Three dimensional printing of polylactic acid (PLA)-wood polysaccharide composite

Authors: Wenyang Xu [a], Andrey Provinch [a], Peter Uppstu [b], Dennis Kronlund [c], Niko Moritz [d], Jarl Hemming [a], Maren Preis [e], Niklas Sandler [e], Willför Stefan [a], Chunlin Xu [a*]

[a]Johan Gadolin Process Chemistry Centre, c/o Laboratory of Wood and Paper Chemistry, Åbo Akademi University, Turku FI-20500, Finland

[b]Laboratory of Polymer Technology, Åbo Akademi University, Turku FI-20500, Finland

[c]Laboratory of Physical Chemistry, Åbo Akademi University, Turku FI-20500, Finland

[d]Department of Prosthetic Dentistry and Biomaterials Science, Institute of Dentistry, University of Turku, Turku FI-20500, Finland

[e]Laboratory of Pharmaceutical Sciences, Åbo Akademi University, Turku FI-20500, Finland

Abstract

Hemicelluloses, the second most abundant polysaccharide right after cellulose, are in practice still treated as a side-stream in biomass processing industries. In the present study, we report an approach to use a wood-derived and side-stream biopolymer, spruce wood hemicellulose (galactoglucomannan) to partially replace the synthetic PLA as feedstock material in 3D printing. A solvent casting approach was developed to ensure the even distribution of the formed binary biocomposites. The blends of hemicellulose and PLA with varied ratio up to 25% of hemicellulose were extruded into filaments by hot melting extrusion. 3D scaffold prototype was successfully printed from the composite filaments by fused deposition modeling 3D printing. Combining with 3D printing technique, the biocompatible and biodegradable feature of spruce wood hemicellulose into the composite scaffolds would definitely boost this new composite material in various biomedical applications such as tissue engineering and drug-eluting scaffolds.

Keywords: Wood biopolymer, 3D printing, Polysaccharides, Galactoglucomannan (GGM), Polylactic acid (PLA), scaffold

1. Introduction

Rapid prototyping (RP), also known as three-dimensional (3D) printing or additive manufacture (AM), has been well developed and adopted in many fields, such as construction, aerospace, healthcare and so on. In RP technique, a complex, high-resolution, and reproducible construct could be rapidly fabricated through a computer-aided design (CAD) model and computer

controlled software. Thus, in particular for fabrication of biomedical devices, RP techniques offers attractive advantages, since customized implants or tissue engineering scaffolds can be designed according to the patient's own 3D medical computed tomography (CT) scan and even very complex structure can be fabricated to meet the individual needs .[1] Among the RP techniques, fused deposition modeling (FDM) has shown greatest versatility by nozzle-deposition-based extrusion with the utilization of biodegradable polymers, including acrylonitrile butadiene styrene (ABS),[2] polylactic acid (PLA),[3-6] poly(ε-caprolactone) (PCL),[7-8] polyvinyl alcohol(PVA),[9] and polyamides (Nylon).[10] Currently, PLA is the main desktop 3D printer feedstock material, owing to its superior mechanical property and thermoplastic processability as well as the green feature of its synthesis routes from renewable resources.

PLA is a linear biopolyester, which is synthesized via ring-opening polymerization of lactide (cyclic di-ester of lactic acid) or polycondensation of lactic acid monomers.[11] In industry, lactic acid is predominantly produced via fermentation of sugars from vast bio resources (mainly corn starch). PLA shows good biocompatibility in physiological conditions and is biodegradable through hydrolytic degradation as well as bioresorbable with its end degradation product being metabolized through lactic acid cycles in vivo.[12] Thus, PLA has found extensive applications in fabricating the biomedical devices, including surgical sutures, orthopedic fixation implants, drug delivery systems, and tissue engineering scaffolds. [13]

However, on one hand, the synthesis of PLA involves the use of catalyst and is also not simple to execute due to the rigorous control of reaction conditions, e.g., temperature, pressure, and pH, which also implies high energy consumption.[14] On the other hand, the popularity use of corn-based PLA has also raised the ethical concern on the global food crisis. To address this, it is deemed as a good strategy to blend natural polymers, for example, polysaccharides with PLA. [15-17]

Hemicelluloses are the second most abundant polysaccharide after cellulose. Galactoglucomannan (GGM) is the major hemicellulose type in softwoods.[18] It accounts for up to 25% in Norway spruce species. In the last two decades, different approaches have been developed to isolate GGM from pulping process as a waste stream where using softwoods as feedstock and from wood chips using hot water extraction.[17] A recent developed technology utilizes vacuum and a design enables water-soluble and polymeric hemicelluloses to be extracted at almost 100% yield from commercial wood chips and at much lower temperature (<150°C) than conventional hot-water extractions or autohydrolysis processes.[19] This makes hemicelluloses promising as cost effective biomaterials.[15-17] Moreover, a wide range of modification routes have been developed ascribed to their copious hydroxyl groups.[20-23] GGM and other hemicelluloses can thus find a broad spectrum of applications as such or after modification, such as, in food and paint formulations, packaging and barrier materials, health

care, and structural composites to replace oil-based products.[15, 24-25] GGM has also been confirmed no cytotoxicity as a biomaterial in both cell culture and wound dressing application.[26-27] Yet, due to the intrinsic structural features of not being thermoplasticizable and possessing complex structure, hemicelluloses cannot undergo the same fabrication processes as synthetic oil-based polymers and thus their commercialization potential is severely undermined.

Hereby, within the concept of 3D printing feedstock material, we propose an approach to use a wood-derived and side-stream biopolymer, GGMs from Norway spruce wood to partially replace the synthetic PLA in 3D printing constructs and investigate the RP feasibility. Polysaccharides offer three potential reaction sites at C-2, C-3 and C-6 that offer untapped potential to incorporate functionality. Chitosan and cellulose have been blended with PLA as 3D printing materials to enhance the desired characteristics, e.g. antimicrobial property and mechanical strength.[28-29] So far, there are no studies to investigate the feasibility of utilizing hemicelluloses as feedstock materials for FDM printing.

In the present study, we report for the first time the 3D printing of PLA/wood hemicellulose composites. A solvent casting approach was developed to ensure the even distribution of the formed binary biocomposites (**Scheme 1**). The blends of GGM and PLA with varied ratio up to 25% of wood hemicellulose were extruded into filaments by hot melting extrusion. Chemical, thermal and mechanical properties of the composites and macroscopic properties of the printed scaffolds were elaborately studied. The printability of the polysaccharide-containing feedstock materials was successfully demonstrated, which offers a new route to apply wood biopolymer in bioplastics for versatile applications in, but not limited to, biomedical devices.

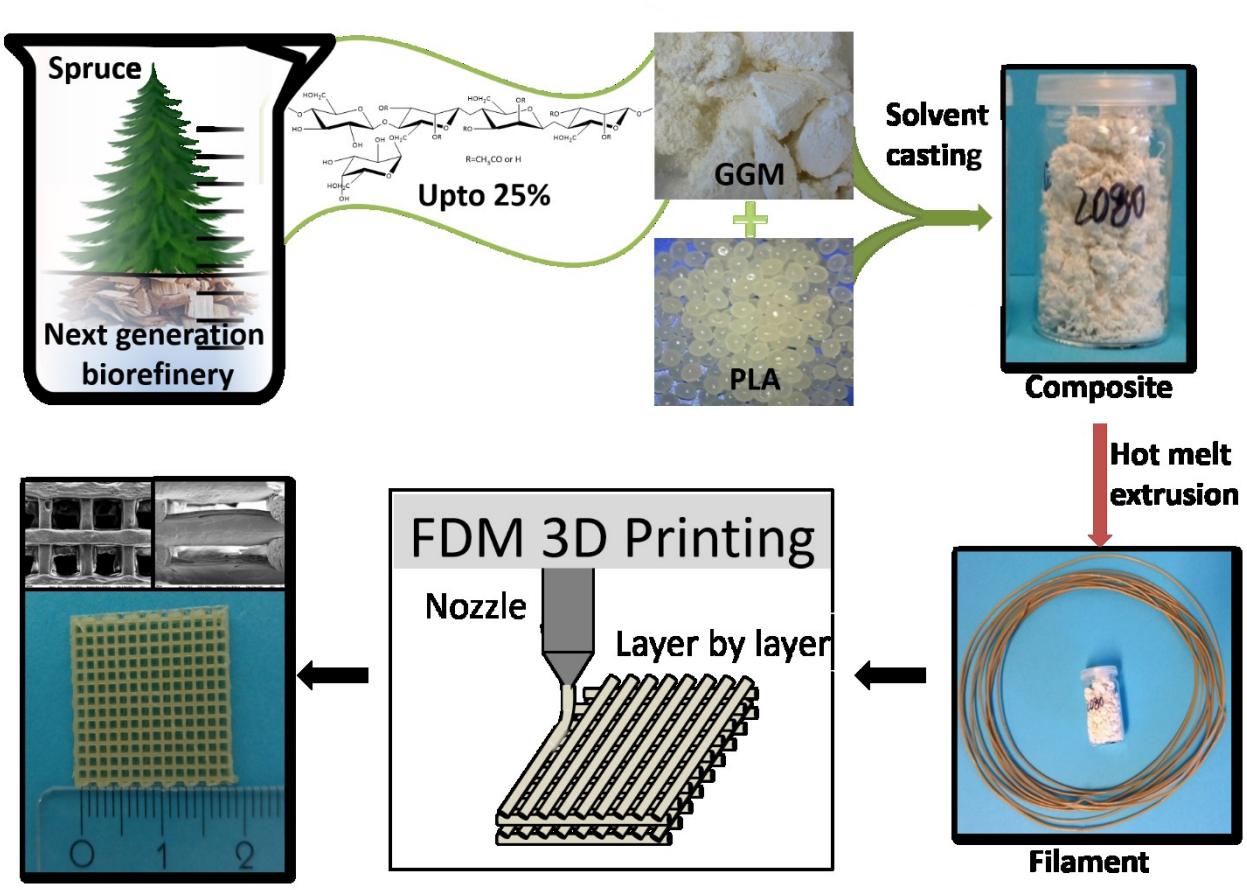

Scheme 1. Schematic Illustration of preparation of composite of GGM and PLA, filaments, and thereof scaffolds by FDM 3D printing. An example for composite ratio of 20:80 in weight of GGM and PLA is shown.

2. Results and discussion

Composite preparation and filament extrusion

A solvent blending method was developed to obtain a homogenous blend of PLA and GGM. GGM and PLA possessing different polarity were not able to be dissolved in the same solvent. Thus, a solvent mixture was developed. DMSO was firstly applied to dissolve GGM and then formed a co-solvent system with DCM. Composite of PLA and GGM was precipitated by subjecting the blend dispersions dropwise the cold ethanol (4 °C).

The dried blends were extruded into filaments by HME with a single screw extruder as displayed in **Figure 1**. Different temperatures were tested and at 165 °C filament with stable shape was formed from the blends. Meanwhile, relatively low temperature resulted in less degradation during the heating process. It can also be seen the color of composites and their filaments became darker when more GGM was added. This might be caused by the presence of small

amount of aromatic residues in GGM, which easily got oxidized in HME process and caused the coloring of the extruded filaments.[17-18] The obtained filaments with diameter in the range of 1.75±0.15 mm were collected for printing step.

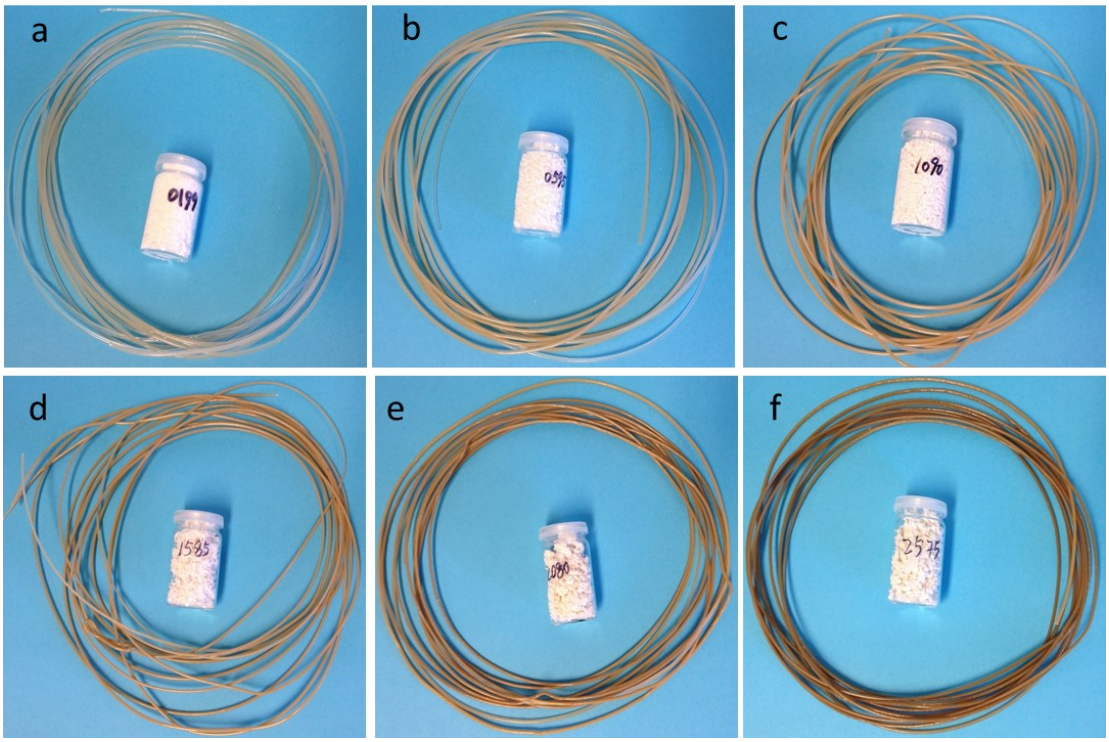

Figure 1. Photographs of blends and filaments: (a) blend 0199 (in bottle) and extruded filament 0199-Fila; (b) blend 0595 and extruded filament 0595-Fila; (c) blend 1090 and extruded filament 1090-Fila; (d) blend 1585 and extruded filament 1585-Fila; (e) blend 2080 and extruded filament 2080-Fila; (f) blend 2575 and extruded filament 2575-Fila

To investigate the structural features of blends before and after extrusion, the starting materials, GGM and PLA pellet, were analyzed by ATR-IR to highlight the differences and peculiarities (shown in **Figure 2a**). The spectrum revealed the abundant hydroxyl group with a broad peak at 3200 cm^{-1} in GGM samples and strong carbonyl C=O stretching around 1750 cm^{-1} with PLA. Moreover, methyl groups bending and stretching at 2954, 2880 and 1383 cm^{-1}, and strong acyl and alkoxy C-O stretching at 1270 and 1050 cm^{-1} were observed in PLA spectrum.[30-31] The peak at 3000 cm^{-1} is associated with the carboxylic acid O-H stretching of the free acid group in PLA. According to the previous study[30], IR spectra with blends and filaments were normalized by 1452 cm^{-1} and the peak at 1750 cm^{-1} was further compared to verify the possibility of the esterification between GGM and PLA. First of all, compared with the relevant composite blend,

this absorption peak of the extruded filament shifted to a lower wavenumber and showed a lower peak intensity, as seen in **Figure 2b** and also in the first derivate graph of spectrums for filament 2575-Fila and its blend 2575 (**Figure S1 in Supporting Information**). This can be caused by the chain scission which happened at high temperature in HME process. Secondly, when compare the filaments of different blend ratio, this peak shift from low to high wavenumbers as well as the peak intensity increased with the increased blend ratio of GGM in the composite. This may suggest a possible weak esterification.

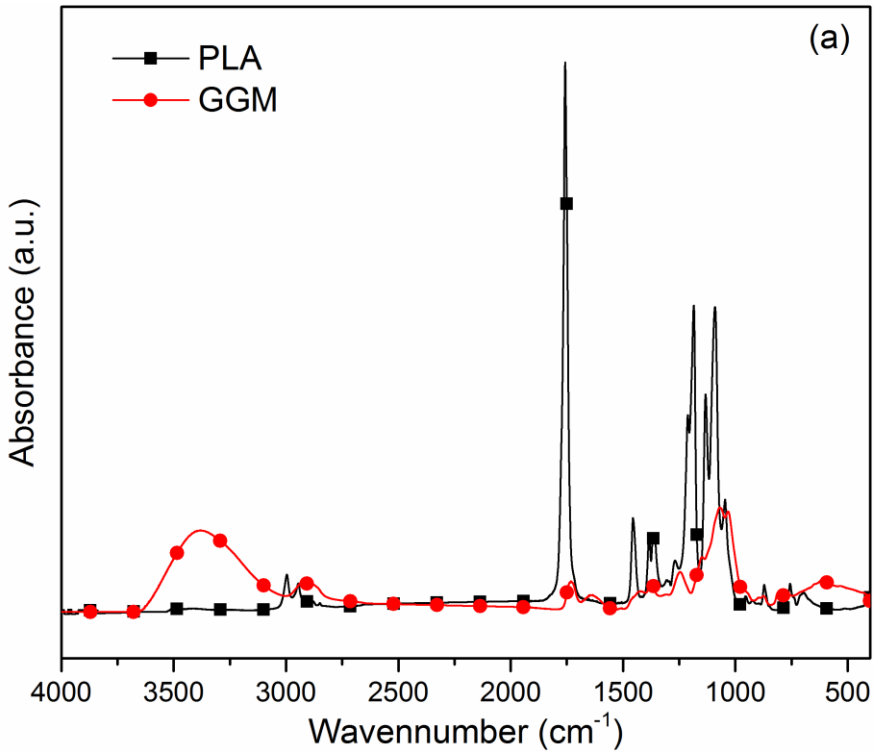

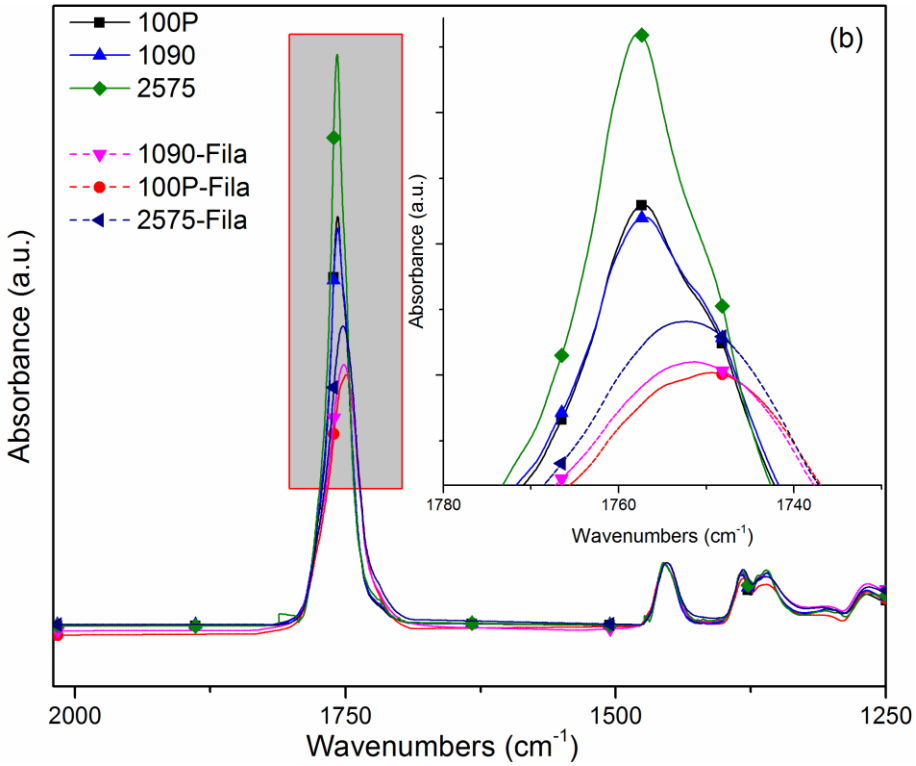

Figure 2. Comparison of FT-IR spectra of PLA and GGM (a); comparison of ATR-FTIR spectra (normalized at 1452 cm-1) of composites and filaments

To further determine the degradation severity for processing blends into filaments in HME (especially PLA), the samples were dissolved in THF for one week, and analyzed by GPC. Here, only PLA could be dissolved in THF for molar mass measurements. In the GPC chromatograms (**Figure 3**), only two peaks belonging to high and low Mw factions of PLA molecules could be observed, which indicates that no obvious structural change of PLA was seen in the HME process.

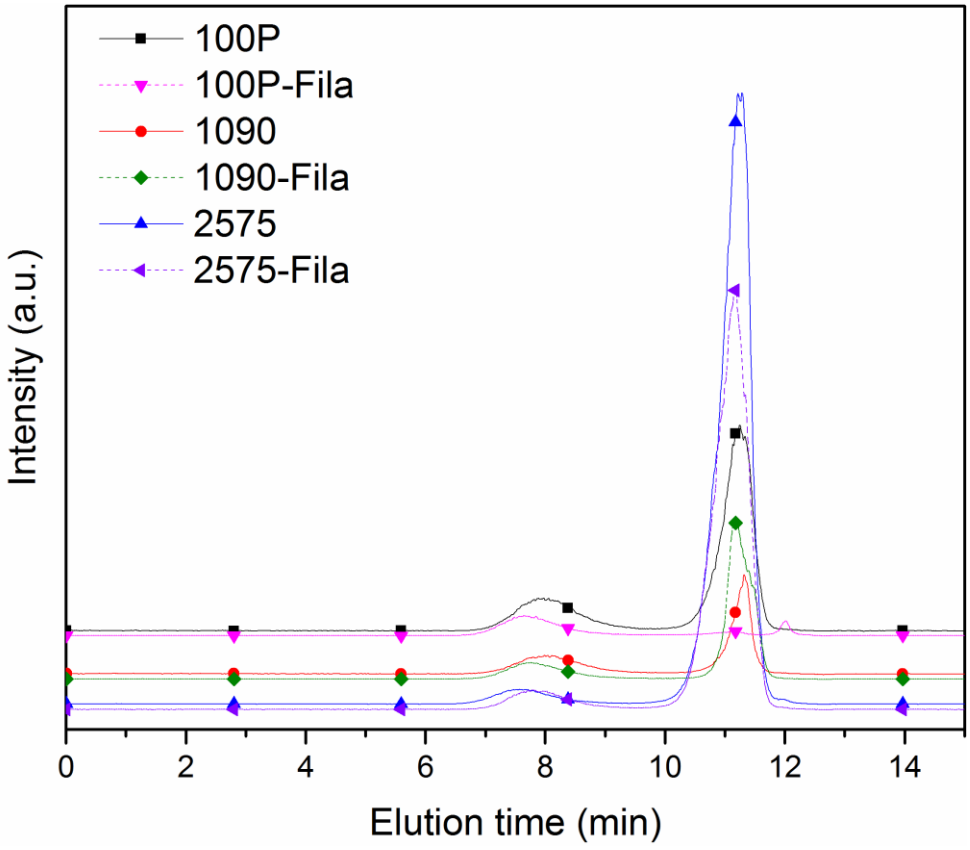

Figure 3. GPC chromatograms of composites with sample 100P, 1090, 2575, and their relative filaments

Thermal property

A heat-cool-heat method was established for DSC analysis. After erasing the thermal history of the investigated materials by the first heating process, the second heating would be more sensitive for detecting the material alterations (**Figure 4a and 4b**), especially for Tg determination. From the second heating run, no significant Tg changes of the blends were detected. In **Figure 4a** and **4b**, only one glass transition temperature (Tg) was detected for each sample in the range of 50-60 °C. It was also observed in the neat PLA samples. Although, a previous study reported that GGM showed the Tg at around 42 °C. Tg of GGM could not be observed here. Thus, the observed Tg points belong to the PLA.[32]

However, the influence of GGM on the melting behavior of the blends is reflected by double melting peak, which is not always visible in the second heating run of the blends (**Figure 4a**). Whereas in second heating thermographs of filament samples (**Figure 4b**), two melting peaks are observed. As seen in **Figure 4b**, the lower melting temperature peaks are more pronounced than the higher temperature peaks. This is probably associated with the melting progression of crystals with different shapes and sizes.[33] In the composite with 25 wt.% GGM (**Figure 4a**), only

one broad melting peak was dominant. This might be due to a fairly broad crystal size distribution of the crystalline phases.[32]

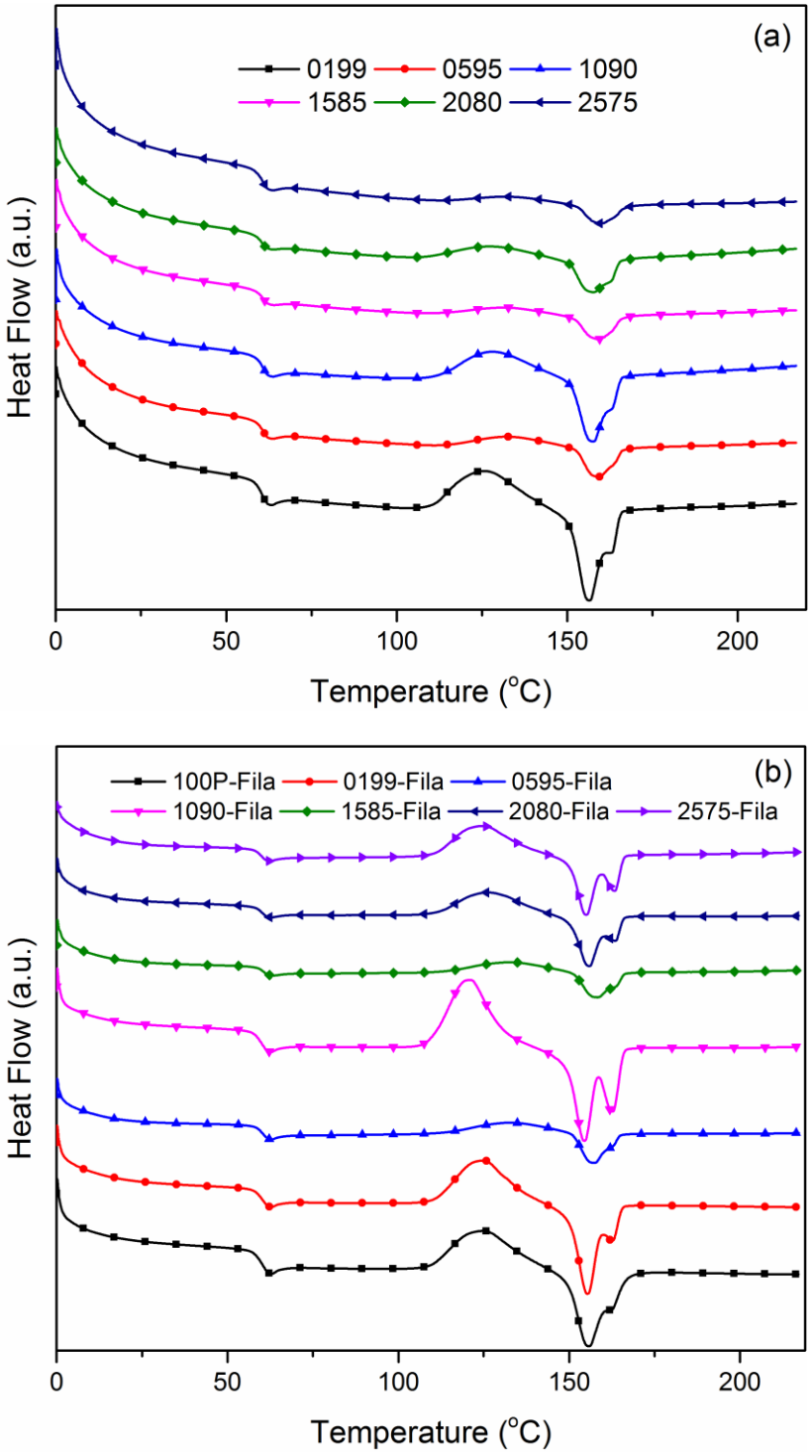

Figure 4. Second heating run of DSC thermograms of blends (a) and filaments (b)

Thethermogravimetric (TG) and first derivative thermogravimetric (DTG) curves of the extruded filaments are shown in **Figure 5** and **Figure S3**, respectively. The neat GGM started degradation at 210 °C. The decomposition of neat PLA started at around 300 °C. Both of these two decomposition temperatures are comparable with previous studies of hemicellulose thermal degradation [34] and PLA thermal degradation behavior.[35] The recorded results showed that the addition of GGM to PLA matrix resulted in a decrease of thermal stability. All the composite filaments started to decompose slightly at quite similar temperatures around 160 °C while the major decomposition took place at temperature higher than 260 °C (**Figure 5**). Slightly higher extrusion temperature at 165 °C and printing temperature at 175 °C were applied to make the melt flow not clogged during extrusion and printing, and less material decomposition.

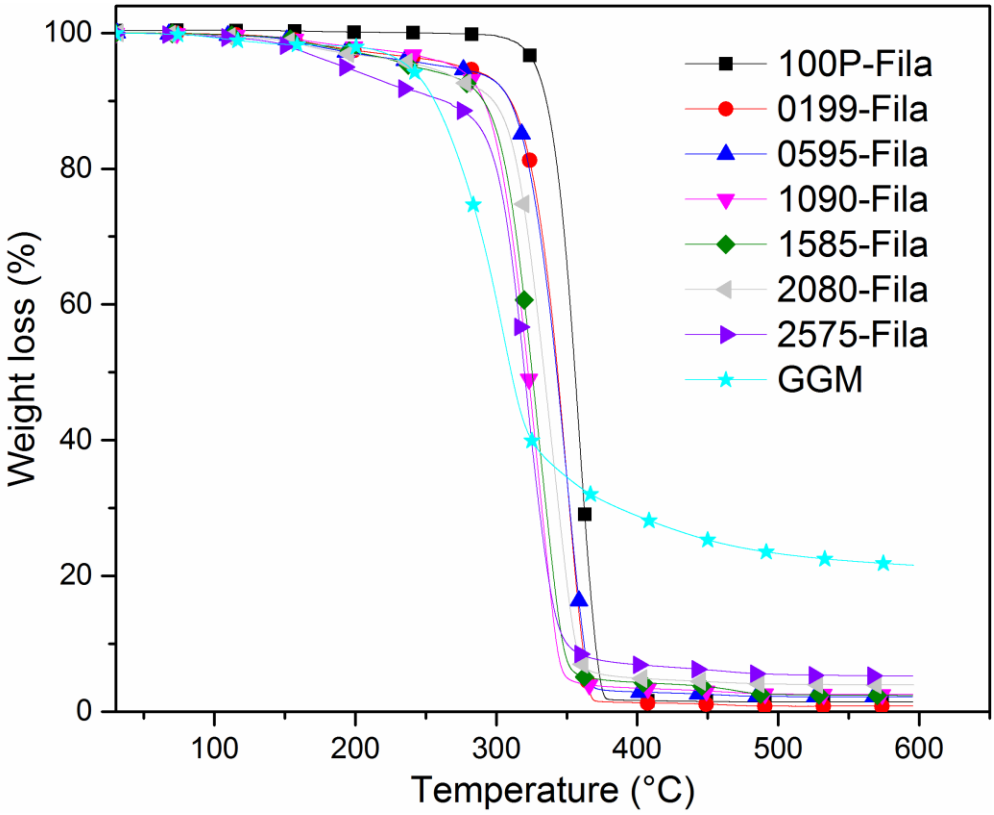

Figure 5. Thermal decomposition curves of filament samples

XRD analysis

Independent crystalline study of the blends and filaments was made by XRD. As shown in the **Figure 6**, the neat PLA exhibited a strong diffraction peak at 16.4°, which can be ascribed to the (020) diffraction. Meanwhile, the other typical peaks at 2θ=15°, 18.5°, and 22.5° were also observed. The blend samples presented similar diffraction patterns like that of the neat PLA

polymer (**Figure S4 in supporting information,**). However, the filaments exhibited peakless patterns with only one broad 'hump'. Thus, no crystalline PLA was present in the extruded filament. HME process, GGM did not act as a nucleating agent for crystalline PLA. Compared with the crystalline blends, the extruded filaments are expected to degrade faster due to their amorphous structure. This probably offers a good alternative to address the concern on the rather long degradation term of PLA, when it is used as implantable devices in biomedical applications.[36-37]

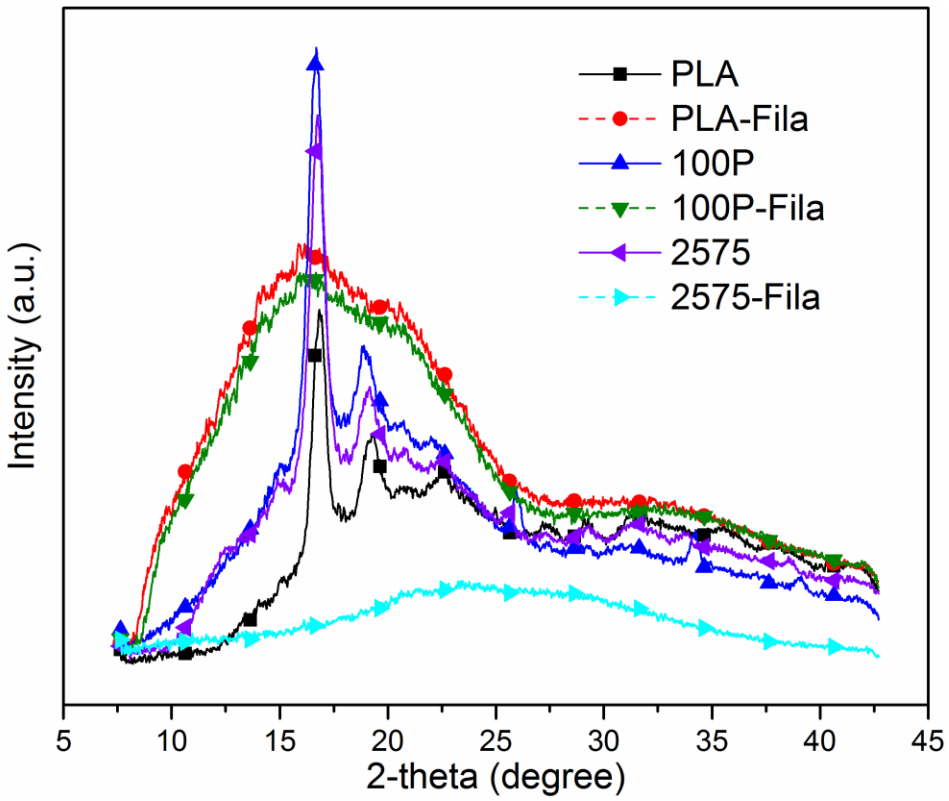

Figure 6. X-ray diffracton pattens for blends and filaments.Note: PLA stands for commercial PLA pellet; PLA-Fila stands for filament directly from PLA pellet.

Rheology and mechanical property

Figure 7a demonstrated the viscosity change of the neat PLA filament and the composite filaments under the applied shear rate at 175 °C. The PLA-Fila, 0199-Fila, and 0595-Fila showed a Newtonian flow at shear rate lower than 5 rad/s. At higher shear rates, the shear thinning property was observed as reported in previous studies of PLA composites.[38-40] The chain interaction between PLA and GGM requires higher shear stress and longer relaxation time.[41] In comparison with the PLA, GGM with amorphous structure has theoretically no melting point. Thus, the behavior of GGM became apparent when low shear rate was applied. At low shear

rate, the GGM molecules could entangle with PLA and could increase the viscosity. Thus, the higher amount of the GGM, the higher the viscosity was. However, the rheological behavior 2575 fell out the predicted trend. This demonstrated that the addition of 20 wt% might be the limit of GGM replacement in PLA melt without modifying the bulk properties of PLA.

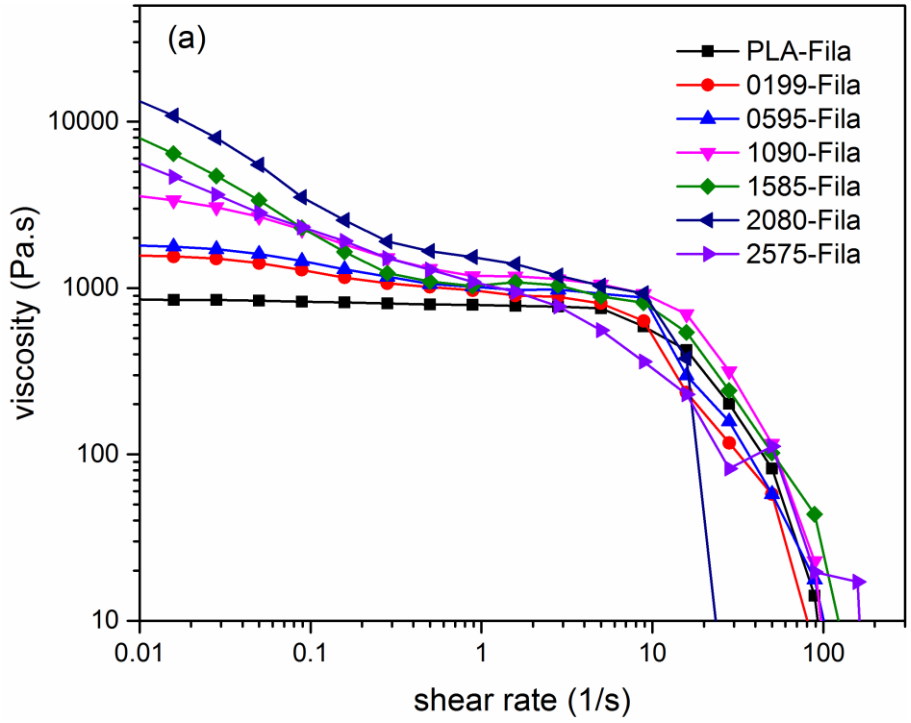

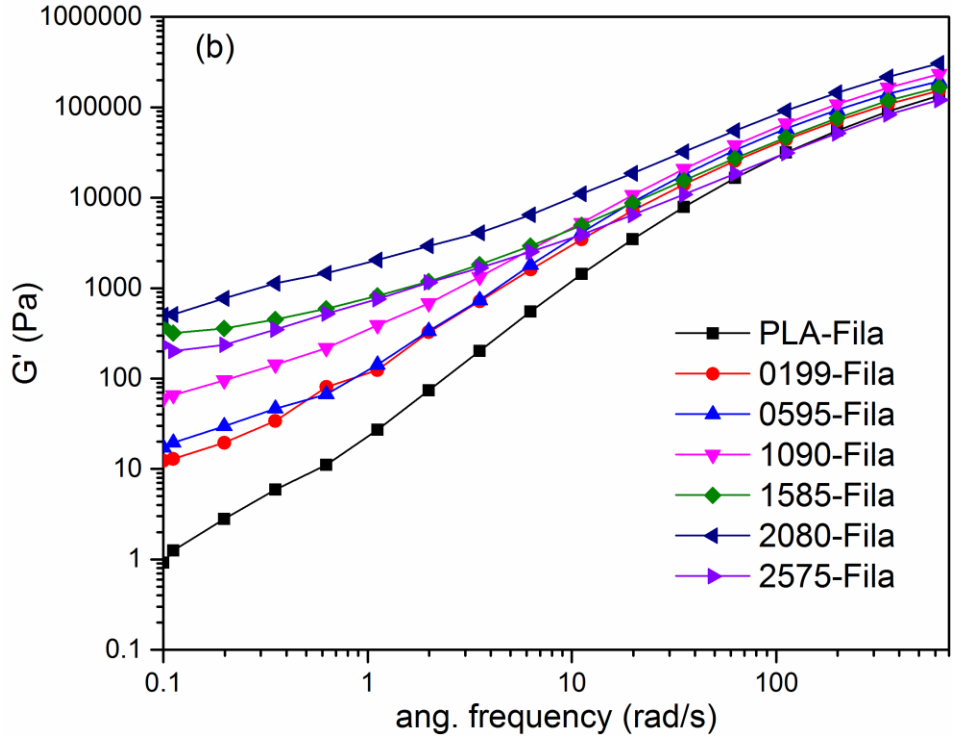

Figure 7. Rheology cures of different filaments at 175 °C (a), and the storage modulus of filaments (b). Note: PLA-Fila stands for filament directly hot melt extruded from commerical PLA pellet.

The elastic modulus curves are shown in **Figure 7b**. The energy storage at the interphase between two components could reveal the elastic property of the composites. As it can be seen, the storage moduli of the composites were higher than the neat PLA. This indicates that GGM and PLA were evenly distributed and their molecule chains are entangled in the composite matrix. This is consistent with the theory that the required relaxation time of the dispersed phase itself is longer than the relaxation of the individual polymer component.[42] Therefore, this behavior is consistent with the observation of the addition of GGM prohibiting the PLA chain's deformation from viscosity curves.

Moreover, the increase in the storage moduli was more notable at a low angular frequency compared with at a high angular frequency (**Figure 7b**). The slope of the storage modulus curves decreased with the increasing amount of GGM. This is also attributed to the longer relaxation time required when a higher amount of GGM was dispersed in PLA melt. The higher proportion of GGM in the composites, the higher storage modulus is seen at the low angular frequencies. At high angular frequencies, whereas, the contribution of PLA was dominating. Thus, less difference was observed at angular frequencies higher than 7 rad/s.

Relevantly, the modulus data is a factor for the measure of the molecular rigidity.[38] As mentioned, the printing process was achieved by melting the filament in liquefier and pushing filament the melted filament through the nozzle, like a piston. During the pushing step, the tendency of the filaments to be bent or buckled is governed by the flexural modulus.[43-44] The value of flexural modulus of GGM blended PLA has a similar flexural modulus (**Figure 8**) compared to the neat PLA around 3.2±0.3 GPa, except that 2575-Fila showed a rather lower value compared with all the other composites. This might be due to the high amount of GGM (25 wt%) impeded the PLA polymer chain entanglement and caused intermolecular phase separation.

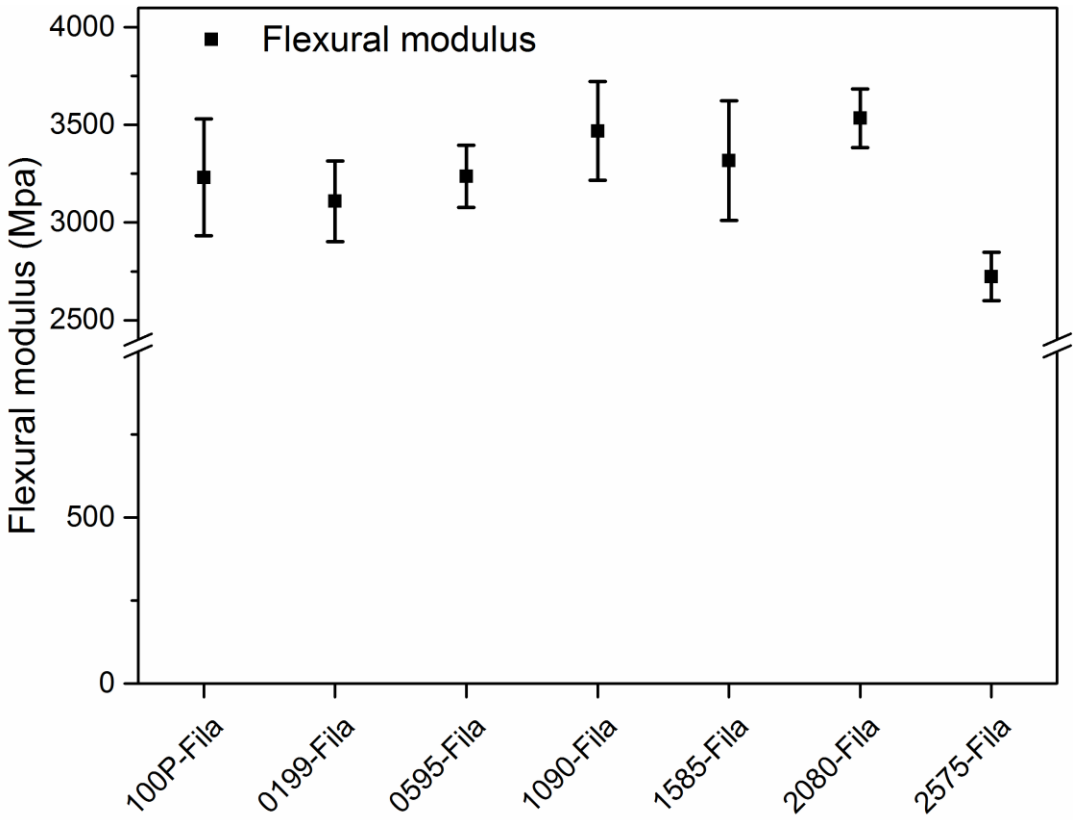

Figure 8. Flexural modulus of filaments from 3 point bending test

3D printing of scaffold prototypes

To our best knowledge, wood hemicelluloses have not been reported to be solely or partially used as a feedstock material for FDM 3D printing yet. Therefore, understanding of the process parameters is crucial for successful printing. The most suitable conditions for printing (listed in **Table 2**) were settled by investigating a few parameters including: 1) diameter of the filament, 2) printing temperature, 3) printing speed, and 4) the mechanical properties of filament.

Firstly, well-controlled filament diameter is essential for printing. Filaments in too small or too big diameter would not be properly grabbed by pinch rollers in the loading process. Discontinuous filament feeding to the liquefier would cause the intermittent extrusion and printing. As investigated, the filament diameter in the range of 1.75±0.15 mm could succeed in printing compared to the default filament diameter of 1.75 mm.

Secondly, the printing temperature is another essential parameter. The heating temperature in the nozzle has an impact on the rheological property of the filaments. The printing temperature used at 175 °C was 10 °C higher than that was used in the filament extrusion process and 30 °C lower than the default 205 °C for commercial PLA filament printing. Essentially, an increase in temperature would cause a decrease in viscosity of the melt state, which could compensate the

less pushing force required compared to that of rotated screw during extrusion. Meanwhile, the applied temperature should be kept far lower from the severe degradation of both components.[34, 45] The ease for a melt to flow under the steady pushing force at 175 °C was assessed by dynamic rheology tests.

With the ease of filament feeding and melt flow, the printing speed was lastly adjusted to achieve better quality of 3D prototypes. In particular, the first layer printing speed plays an important role in determining the quality of printed object. A relatively lower speed at 15 mm/s was used for the first layer printing (**Table 2**). In order to obtain a fine and high-resolution structure, the infill printing speed was also tuned at 20 m/s compared to the speed at 45 mm/s, which is generally used for PLA printing under the same condition.

The surface and structural morphology of filament and 3D printed scaffold of sample 1090-Fila is shown in SEM images (**Figure 9**). The printability of all the other filaments was illustrated by SEM images in the supporting information (**Figure S5-S10**). It reveals that the surface of the scaffolds with more GGM blended became rougher and more porous compared with smooth and compact surface of neat PLA (**Figure S5**).

The blends of GGM and PLA were considered as immiscible blends due to the phase separation, which was also confirmed by SEM image, for instance, in **Figure 9d**. Aggregates could be seen on the printed stripe surface and that are likely to be aggregates of GGM. Moreover, aggregates could be also observed in the bending cross-section image (**Figure 9e**). This is probably due to the aggregation of GGM molecules formed during cooling and solidifying after HME process, where the process temperature of 175 °C is above the PLA melting point. Moreover, GGM polymer chains are prone to self-assemble due to the solubility and polarity parameter differences between PLA and GGM.[46] When the portion of amorphous GGM was higher than 20 wt%, sponge-like phase instead of continuous phase formed by PLA was revealed by the cross-section images (**Figure S9e** and **S10e**). The spongy structure of the filament resulted in the loss of flexural strength.

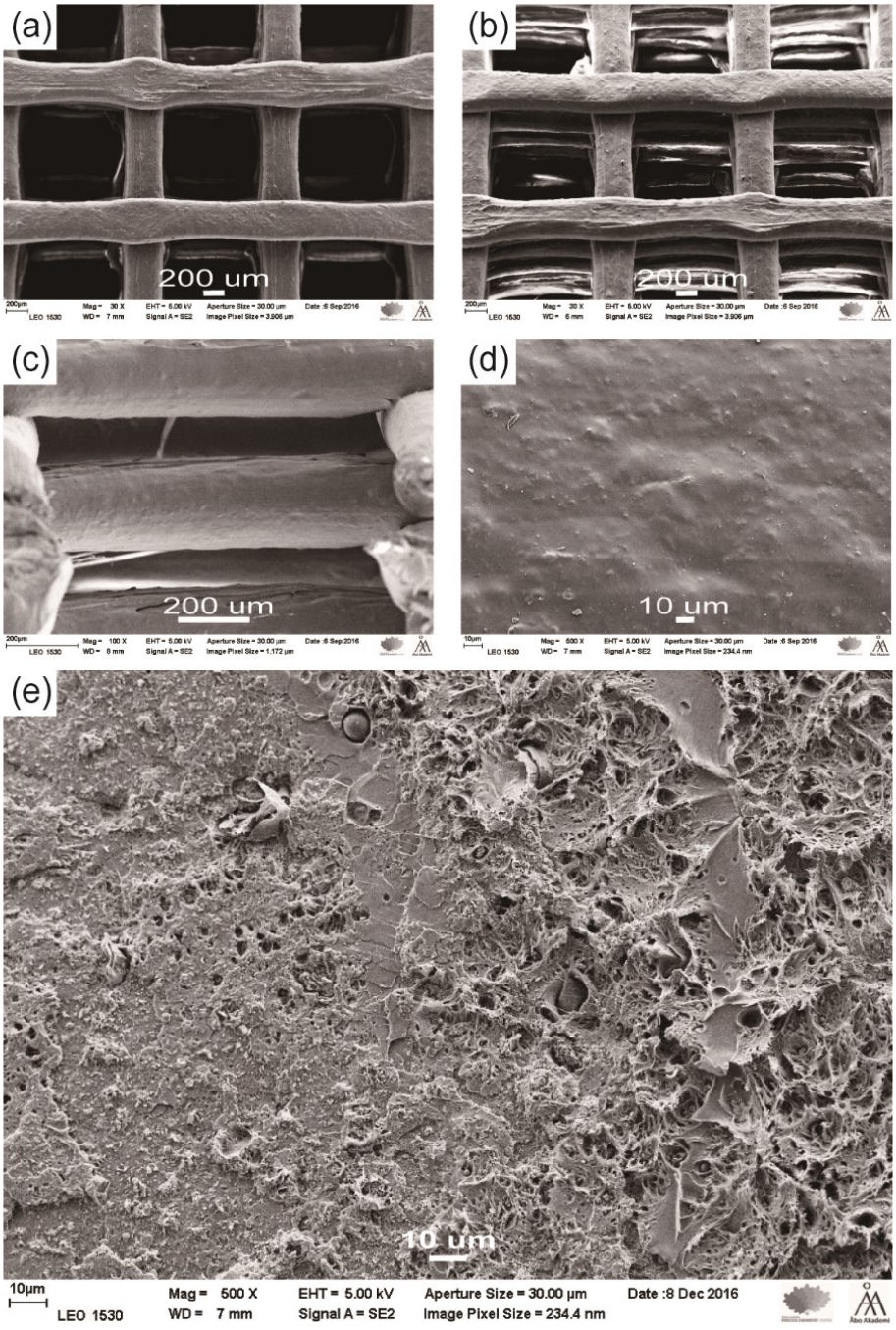

Figure 9.SEM images of 1090-Fila based 3D printed scaffold (a and b),SEM image from side of the scaffold (c), surface image of the 3D printed stripe in the scaffold(d), and bending cross-section images from 1090-Fila (e).

3. Conclusion

In summary, 3D scaffold prototype was successfully printed from composites of PLA with up to 25% wood hemicellulose for the first time. A solvent casting approach was developed to achieve binary biocomposites with even distribution of PLA and GGM. The composites were extruded to filaments followed by FDM 3D printing. When crystallized PLA was replaced by up to 20% amorphous GGM, the composites could still keep the mechanical property.

It is worth to stress that rational of biorefinery; technologies are available to supply hemicelluloses with a large volume, however, the application of hemicelluloses as bioplastic is still undermined. We have demonstrated a new route to use such side-stream and biorenewable wood biopolymer as feedstock materials for FDM 3D printing. On one hand, incorporation of wood hemicelluloses may reduce the application of PLA; on the other hand, hemicelluloses with versatile active sites may be used as carriers or molecular anchors to introduce desired functionality and features. The printed objects have significant potential in numerous applications, but not limited to, biomedical devices where physical and chemical cues are needed to satisfy the tissue engineering requirements.

Acknowledgement

Ms. Sonja Granith and Mr. Humayun Aziz from the Laboratry of Polymer technology in Åbo Akademi University, Finland, are thanked by the authors for their great help with rheological and mechanical properties analyses, respectively. Dr. Xiaoju Wang from Laboratory of Inorganic Chemistry is thanked for reading through the manuscript and valuable discussions. This work is also part of activity within Johan Gadolin Process Chemistry Centre, the Center of Excellence appointed by Åbo Akademy University during 2015-2018.

4. Experimental Section

4.1 Materials

Polylactic acid (PLA, Ingeo™ biopolymer 4043D) pellets were purchased from NatureWork, USA. Galactoglucomanans (GGM) were isolated with hot water extraction as previously reported.[16] Dichlorimathane (DCM) and Dimethyl sulfoxide (DMSO, technical grade) were purchased from VWR and Sigma-Aldrich, respectively. Ethanol (technical grade) was supplied from Altia Oy, Finland.

4.2 PLA and GGM composite preparation

In order to obtain an evenly distributed composite, a solvent blending method was developed. Different ratios between GGM and PLA were tuned as shown in **Table 1.** GGM was firstly dissolved in DMSO at 40 °C. DCM (80%) was added after GGM had dissolved. PLA pellets were then added. Ultrasonification with 15 min was applied with a VWR ultrasonic cleaner (600 W) to ensure homogeneous mixing. The blends in the solvent mixture of DMSO and DCM were stirred

at 35 °C overnight. Afterwards, the blends were precipitated by adding into cold ethanol (the volume fraction between solvent and ethanol was 1:9). All the precipitates were collected and further dried in vacuum desiccator (D-6450 Hanau, Heraeus) at 40 °C.

Table 1. Blending ratio between GGM and PLA, and the composite preparation condition

Blend codes#	GGM (wt.%)	PLA (wt.%)	Solvent*
100P	0	100	DMSO:DCM 20:80
0199	1	99	
0595	5	95	
1090	10	90	
1585	15	85	
2080	20	80	
2575	25	75	

the composites from solvent blending are coded according to the list and thereafter extruded filaments with suffix '-Fila' in the manuscript; *Concentration of 10 g solid material per 100 mL solvent mixture was kept for all the solvent blending processes.

4.3 Hot-melt extrusion (HME) and 3D printing with the FDM™ technique

Filaments were extruded by hot-melt extrusion with **NOZTEK pro extruder (UK)** at 165 °C with a nozzle diameter of 1.7 mm after screening at different temperatures ranging from 150 °C to 185 °C.

The scaffold prototypes were designed and printed by the control of 'MatterControl' software as the stereolithography files (.stl). The screenshot of the prototype in MatterControl is shown in **Figure S11**. The dimensions of IUS were 20 mm in length, 20 mm in width, and 2 mm in height (10 layers). A Me3D desktop printer (Australia), based on the FDM™, was used for 3D printing of the above-mentioned prototypes. The printing parameters are reported in **Table 2**.

Table 2. 3D printing parameters

Printing temperature	175 °C
Layer height	200 µm
Infill density	30%
Infill type	Line
Layer angle	90 °
Printing speed	First layer: 15 mm/s Infill: 20 mm/s
Nozzle diameter	400 µm

4.4 Characterization

4.4.1 Attenuated total reflectance-infrared spectroscopy (ATR-FTIR)

The composites and HME filaments were analyzed by Thermo ScientificTM NicoletTM iSTM 50 FTIR Spectrometer (United States). The spectra were collected with ATR mode in the absorbance mode from an accumulation of 64 scans at a 4 cm^{-1} resolution in the range of 4000-400 cm^{-1}. If not differently specified, the spectra were normalized to the peak at 1452 cm^{-1}.

4.4.2 Gel permeation chromatography (GPC)

GPC analyses were conducted using a Shimadu setup. One percent of acetic acid in THF was used as eluent at flow rate of 0.8 mL/min with a column packed with X-stream H20 Mixed bed from JORDI, USA. One gram of composites or filaments was dissolved in 10 mL of THF. Ultrasonic sound with Less than 15 seconds was applied every 12 hours to enhance the sample solubility. All the samples were shaken for one week. Each 0.5 mL dissolved samples was filtered with 0.2 µm nylon filters before injection.

Molar mass analysis was conducted using a standard gel permeation chromatography (GPC) technique calibrated with polystyrene standard.

4.4.3 Differential scanning calorimetry (DSC)

The composite samples were run as a conventional DSC (DSC Q 2000, TA instruments, USA) in a heat/cool/heat cycle at a temperature range of 0 °C to 220 °C with a heating and cooling rate of 10 °C/min in a standard aluminum pan. Nitrogen was used as a purge gas with a flow rate of 50 ml/min. Samples of 3 ± 1 mg for composites and filaments were used. The thermograms were analyzed with the TA Instruments Universal 2000 Software.

4.4.4 Thermogravimetric analysis (TGA)

The thermal stability of composites and filaments was investigated by a Thermal Gravimetric Analyser (Q600, TA instruments). The samples were pre-dried under 40 °C vacuum desiccator before thermal analysis. The heating rate in the experiment was 10 °C/min from room temperature up to 600 °C under nitrogen.

4.4.5 X-ray diffraction (XRD)

X-ray diffraction (XRD) was performed with a Bruker D8 Discovery (Bruker-AXS, Karlsruhe, Germany) using CuKα radiation (λ = 1.54184 nm), a 0.5-mm collimator, a Göbel mirror and a 2D HI-STAR© detector. The XRD spectra were collected in the 2ϑ range of 7.6°–42.7° using a 2D Hi-Star detector measuring frames using 600 s/frame. The X-ray tube was operated at 40 kV and 40 mA.

4.4.6 Rheology

Rheology measurements were carried out to determine the shear viscosity profile filaments at the printing temperature of 175 °C (the printing temperature). The measurements were conducted with a rotational AR 2000 rheometer (TA instruments, USA), using a parallel plate geometry at the shear rate of 0.005 to 200 s^{-1}. The geometry of the plates and the gap between them were 15 and 1 mm, respectively. The sample size was around one gram.

4.4.7 Mechanical strength

Mechanical tests in terms of flexural strength were performed. Flexural strength was studied by three–point–bending test according to *ASTM D790* standard method. The filaments with diameter around 1.75±0.15 mm were cut to 30 mm long for flexural test using a LLOYD LR30K plus instrument operated at crosshead speed of 10 mm/min.

4.4.8 Scanning electron microscopy (SEM)

A scanning electron microscope (SEM LEO Gemini 1530 with a ThermoNORAN Vantage X-ray analysing system manufactured by Thermo Scientific, Germany) was used to obtain the images of surface morphology of the samples. A thin carbon coating was applied onto the sample to make it more electrically conductive. The microscope was operated in a secondary electron mode at an accelerating voltage of 2.7 kV for imaging with an aperture size of 60 µm. The cross-section after bending measurements was also analyzed by SEM.

References

1. Hollister, S. J., Porous scaffold design for tissue engineering. *Nature materials* **2005,** *4* (7), 518-524.
2. Rocha, C. R.; Perez, A. R. T.; Roberson, D. A.; Shemelya, C. M.; MacDonald, E.; Wicker, R. B., Novel ABS-based binary and ternary polymer blends for material extrusion 3D printing. *Journal of Materials Research* **2014,** *29* (17), 1859-1866.
3. Matsuzaki, R.; Ueda, M.; Namiki, M.; Jeong, T.-K.; Asahara, H.; Horiguchi, K.; Nakamura, T.; Todoroki, A.; Hirano, Y., Three-dimensional printing of continuous-fiber composites by in-nozzle impregnation. *Scientific reports* **2016,** *6*.
4. Davidson, J. R.; Appuhamillage, G. A.; Thompson, C. M.; Voit, W.; Smaldone, R. A., Design Paradigm Utilizing Reversible Diels–Alder Reactions to Enhance the Mechanical Properties of 3D Printed Materials. *ACS applied materials & interfaces* **2016,** *8* (26), 16961-16966.
5. Almeida, C. R.; Serra, T.; Oliveira, M. I.; Planell, J. A.; Barbosa, M. A.; Navarro, M., Impact of 3-D printed PLA-and chitosan-based scaffolds on human monocyte/macrophage responses: unraveling the effect of 3-D structures on inflammation. *Acta biomaterialia* **2014,** *10* (2), 613-622.
6. Sandler, N.; Salmela, I.; Fallarero, A.; Rosling, A.; Khajeheian, M.; Kolakovic, R.; Genina, N.; Nyman, J.; Vuorela, P., Towards fabrication of 3D printed medical devices to prevent biofilm formation. *International Journal of Pharmaceutics* **2014,** *459* (1–2), 62-64.

7. Seyednejad, H.; Gawlitta, D.; Dhert, W. J. A.; van Nostrum, C. F.; Vermonden, T.; Hennink, W. E., Preparation and characterization of a three-dimensional printed scaffold based on a functionalized polyester for bone tissue engineering applications. *Acta Biomaterialia* **2011,** *7* (5), 1999-2006.
8. Holländer, J.; Genina, N.; Jukarainen, H.; Khajeheian, M.; Rosling, A.; Mäkilä, E.; Sandler, N., Three-dimensional printed PCL-based implantable prototypes of medical devices for controlled drug delivery. *Journal of pharmaceutical sciences* **2016**, 105(9):2665-76.
9. Goyanes, A.; Buanz, A. B. M.; Basit, A. W.; Gaisford, S., Fused-filament 3D printing (3DP) for fabrication of tablets. *International Journal of Pharmaceutics* **2014,** *476* (1–2), 88-92.
10. Novakova-Marcincinova, L.; Novak-Marcincin, J.; Barna, J.; Torok, J. In *Special materials used in FDM rapid prototyping technology application*, 2012 IEEE 16th International Conference on Intelligent Engineering Systems (INES), IEEE: **2012**; pp 73-76.
11. Lee, C.; Hong, S., An Overview of the Synthesis and Synthetic Mechanism of Poly (Lactic acid). *Modern Chemistry & Applications* **2013,** 2:144. doi: 10.4172/2329-6798.1000144.
12. Maurus, P. B.; Kaeding, C. C., Bioabsorbable implant material review. *Operative Techniques in Sports Medicine* **2004,** *12* (3), 158-160.
13. Tanase, C. E.; Spiridon, I., PLA/chitosan/keratin composites for biomedical applications. *Materials Science and Engineering: C* **2014,** *40*, 242-247.
14. Lasprilla, A. J.; Martinez, G. A.; Lunelli, B. H.; Jardini, A. L.; Maciel Filho, R., Poly-lactic acid synthesis for application in biomedical devices—A review. *Biotechnology advances* **2012,** *30* (1), 321-328.
15. Willför, S.; Sundberg, K.; Tenkanen, M.; Holmbom, B., Spruce-derived mannans – A potential raw material for hydrocolloids and novel advanced natural materials. *Carbohydrate Polymers* **2008,** *72* (2), 197-210.
16. Xu, C.; Willfor, S.; Sundberg, K.; Pettersson, C.; Holmbom, B., Physico-chemical characterization of spruce galactoglucomannan solutions: stability, surface activity and rheology. *Cellulose Chemistry and Technology* **2007,** *41* (1), 51.
17. Willför, S.; Rehn, P.; Sundberg, A.; Sundberg, K.; Holmbom, B., Recovery of water-soluble acetylgalactoglucomannans from mechanical pulp of spruce. *Tappi Journal* **2003,** *2* (11), 27-32.
18. Willför, S.; Sjöholm, R.; Laine, C.; Roslund, M.; Hemming, J.; Holmbom, B., Characterisation of water-soluble galactoglucomannans from Norway spruce wood and thermomechanical pulp. *Carbohydrate Polymers* **2003,** *52* (2), 175-187.
19. VON, S. S., Method for extracting biomass. Google Patents: **2014**.
20. Albertsson, A.-C.; Voepel, J.; Edlund, U.; Dahlman, O.; Soderqvist-Lindblad, M., Design of renewable hydrogel release systems from fiberboard mill wastewater. *Biomacromolecules* **2010,** *11* (5), 1406-1411.
21. Karaaslan, M. A.; Tshabalala, M. A.; Yelle, D. J.; Buschle-Diller, G., Nanoreinforced biocompatible hydrogels from wood hemicelluloses and cellulose whiskers. *Carbohydrate Polymers* **2011,** *86* (1), 192-201.
22. Kisonen, V.; Eklund, P.; Auer, M.; Sjöholm, R.; Pranovich, A.; Hemming, J.; Sundberg, A.; Aseyev, V.; Willför, S., Hydrophobication and characterisation of O-acetyl-galactoglucomannan for papermaking and barrier applications. *Carbohydrate research* **2012,** *352*, 151-158.
23. Söderqvist Lindblad, M.; Ranucci, E.; Albertsson, A. C., Biodegradable Polymers from Renewable Sources. New Hemicellulose‐Based Hydrogels. *Macromolecular Rapid Communications* **2001,** *22* (12), 962-967.
24. Liu, J.; Willför, S.; Xu, C., A review of bioactive plant polysaccharides: Biological activities, functionalization, and biomedical applications. *Bioactive Carbohydrates and Dietary Fibre* **2015,** *5* (1), 31-61.
25. Petzold-Welcke, K.; Schwikal, K.; Daus, S.; Heinze, T., Xylan derivatives and their application potential–Mini-review of own results. *Carbohydrate polymers* **2014,** *100*, 80-88.

26. Liu, J.; Chinga-Carrasco, G.; Cheng, F.; Xu, W.; Willför, S.; Syverud, K.; Xu, C., Hemicellulose-reinforced nanocellulose hydrogels for wound healing application. *Cellulose* **2016,** *23* (5), 3129-3143.
27. Markstedt, K.; Xu, W.; Liu, J.; Xu, C.; Gatenholm, P., Synthesis of tunable hydrogels based on O-acetyl-galactoglucomannans from spruce. *Carbohydrate Polymers*,*157,* 1349-1357.
28. Wu, C.-S., Modulation, functionality, and cytocompatibility of three-dimensional printing materials made from chitosan-based polysaccharide composites. *Materials Science and Engineering: C* **2016,** *69*, 27-36.
29. Murphy, C. A.; Collins, M. N., Microcrystalline cellulose reinforced polylactic acid biocomposite filaments for 3D printing. *Polymer Composites* **201,** doi: 10.1002/pc.24069.
30. Signori, F.; Boggioni, A.; Righetti, M. C.; Rondán, C. E.; Bronco, S.; Ciardelli, F., Evidences of Transesterification, Chain Branching and Cross‐Linking in a Biopolyester Commercial Blend upon Reaction with Dicumyl Peroxide in the Melt. *Macromolecular Materials and Engineering* **2015,** *300* (2), 153-160.
31. Wang, D. K.; Varanasi, S.; Fredericks, P. M.; Hill, D. J.; Symons, A. L.; Whittaker, A. K.; Rasoul, F., FT‐IR characterization and hydrolysis of PLA‐PEG‐PLA based copolyester hydrogels with short PLA segments and a cytocompatibility study. *Journal of Polymer Science Part A: Polymer Chemistry* **2013,** *51* (24), 5163-5176.
32. Žepič, V.; Poljanšek, I.; Oven, P.; Čop, M., COST-FP1105: Properties of PLA films reinforced with unmodified and acetylated freeze dried nanofibrillated cellulose. *Holzforschung* **2016,** *70* (12), 1125-1134.
33. Wasanasuk, K.; Tashiro, K., Crystal structure and disorder in Poly (l-lactic acid) δ form (α′ form) and the phase transition mechanism to the ordered α form. *Polymer* **2011,** *52* (26), 6097-6109.
34. Werner, K.; Pommer, L.; Broström, M., Thermal decomposition of hemicelluloses. *Journal of Analytical and Applied Pyrolysis* **2014,** *110*, 130-137.
35. Spiridon, I.; Leluk, K.; Resmerita, A. M.; Darie, R. N., Evaluation of PLA–lignin bioplastics properties before and after accelerated weathering. *Composites Part B: Engineering* **2015,** *69*, 342-349.
36. Lyu, S.; Untereker, D., Degradability of polymers for implantable biomedical devices. *International journal of molecular sciences* **2009,** *10* (9), 4033-4065.
37. Wang, Z.; Wang, Y.; Ito, Y.; Zhang, P.; Chen, X., A comparative study on the in vivo degradation of poly (L-lactide) based composite implants for bone fracture fixation. *Scientific reports* **2016,** *6*, 20770. doi: 10.1038/srep20770.
38. Shumigin, D.; Tarasova, E.; Krumme, A.; Meier, P., Rheological and mechanical properties of poly (lactic) acid/cellulose and LDPE/cellulose composites. *Materials Science* **2011,** *17* (1), 32-37.
39. Al-Itry, R.; Lamnawar, K.; Maazouz, A., Biopolymer blends based on poly (lactic acid): shear and elongation rheology/structure/blowing process relationships. *Polymers* **2015,** *7* (5), 939-962.
40. Al-Itry, R.; Lamnawar, K.; Maazouz, A., Improvement of thermal stability, rheological and mechanical properties of PLA, PBAT and their blends by reactive extrusion with functionalized epoxy. *Polymer Degradation and Stability* **2012,** *97* (10), 1898-1914.
41. Lozano, K.; Bonilla‐Rios, J.; Barrera, E., A study on nanofiber‐reinforced thermoplastic composites (II): Investigation of the mixing rheology and conduction properties. *Journal of Applied Polymer Science* **2001,** *80* (8), 1162-1172.
42. Han, C. D., *Rheology and Processing of Polymeric Materials: Volume 1: Polymer Rheology*. Oxford University Press on Demand: **2007**; Vol. 1.
43. Genina, N.; Holländer, J.; Jukarainen, H.; Mäkilä, E.; Salonen, J.; Sandler, N., Ethylene vinyl acetate (EVA) as a new drug carrier for 3D printed medical drug delivery devices. *European Journal of Pharmaceutical Sciences* **2016,** *90*, 53-63.
44. Comb, J. W.; Priedeman, W. R.; Turley, P. W. In *FDM technology process improvements*, Proceedings of Solid Freeform Fabrication Symposium, DTIC Document: **1994**; pp 42-49.

45. Kopinke, F.-D.; Remmler, M.; Mackenzie, K.; Möder, M.; Wachsen, O., Thermal decomposition of biodegradable polyesters—II. Poly (lactic acid). *polymer Degradation and Stability* **1996,** *53* (3), 329-342.
46. He, N.; Smeds, A.; Friman, R.; Rosenholm, J. B., Solubility parameters of biopolymers. *Physics and Chemistry of Liquids* **2013,** *51* (3), 302-316.

Title: Novel FDM 3D-Printing biomaterial from Norway spruce Galactoglucomannans and PLA

Authors: Wenyang Xu [a], Andrey Provinch [a], Peter Uppstu [b], Dennis Kronlund [c], Niko Moritz [d], Jarl Hemming [a], Niklas Sandler [e], Willfor Stefan [a], Chunlin Xu [a*]

[a]Johan Gadolin Process Chemistry Centre, c/o Laboratory of Wood and Paper Chemistry, Åbo Akademi University, Turku FI-20500, Finland

[b]Laboratory of Polymer Technology, Åbo Akademi University, Turku FI-20500, Finland

[c]Laboratory of Physical Chemistry, Åbo Akademi University, Turku FI-20500, Finland

[d]Department of Prosthetic Dentistry and Biomaterials Science, Institute of Dentistry, University of Turku, Turku FI-20500, Finland

[e]Laboratory of Pharmaceutical Sciences, Åbo Akademi University, Turku FI-20500, Finland

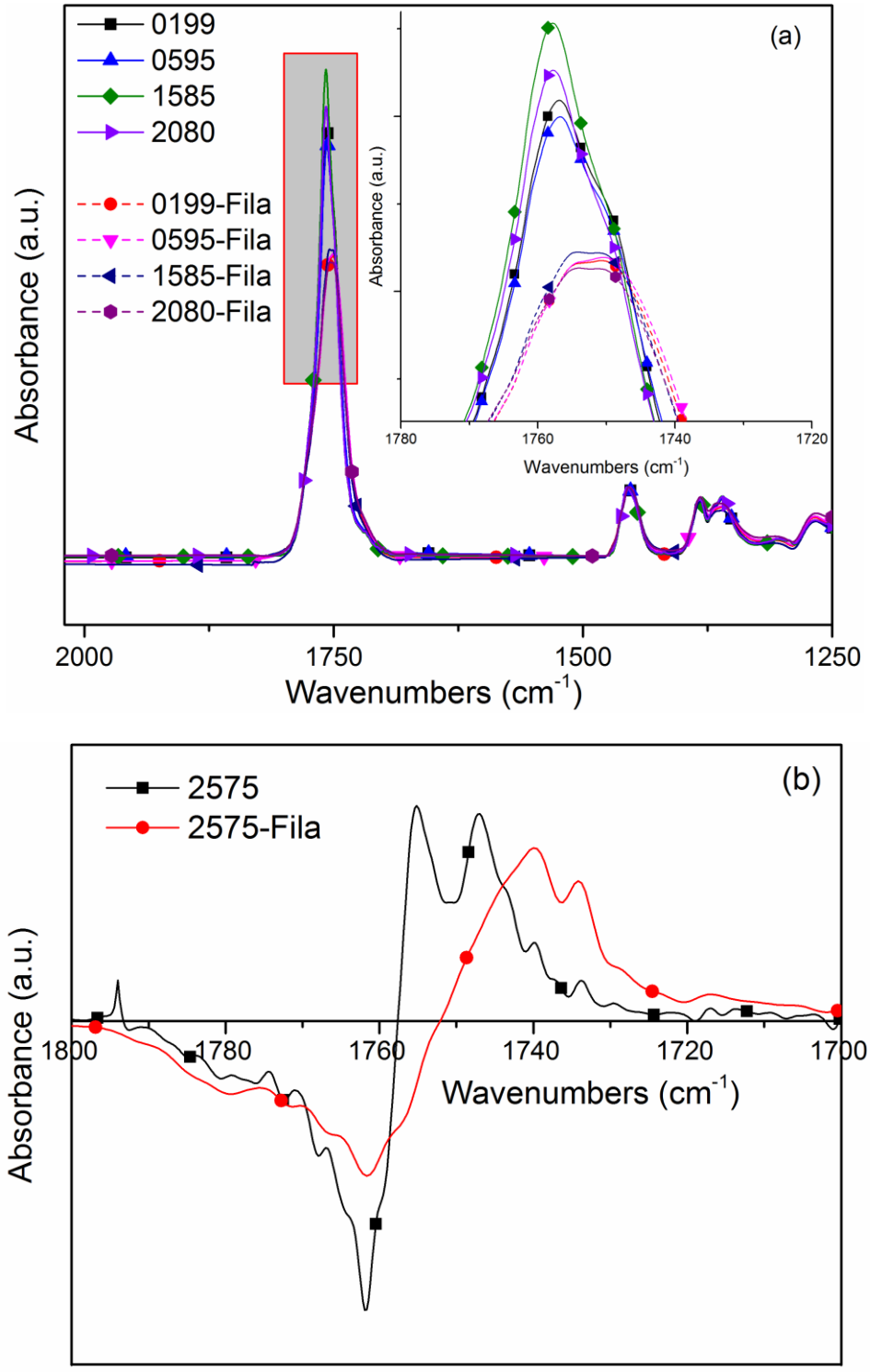

Figure S1. Normalized ATR-FTIR spectra (up), and first derivative ATR-FTIR spectra of the 2575-C and 2575-F demonstrating the peak differences among the wavenumbers between 1700-1800 cm^{-1} (down)

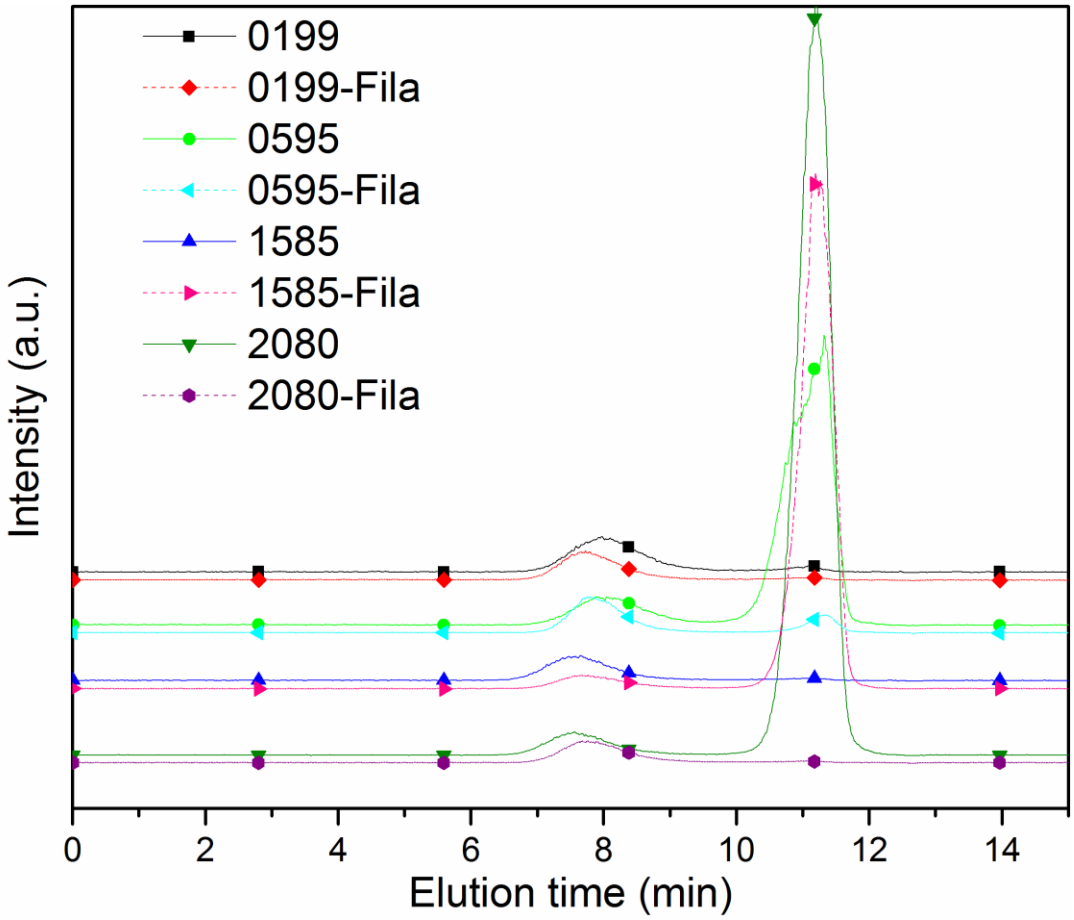

Figure S2. GPC chromatograms with both blends and filaments

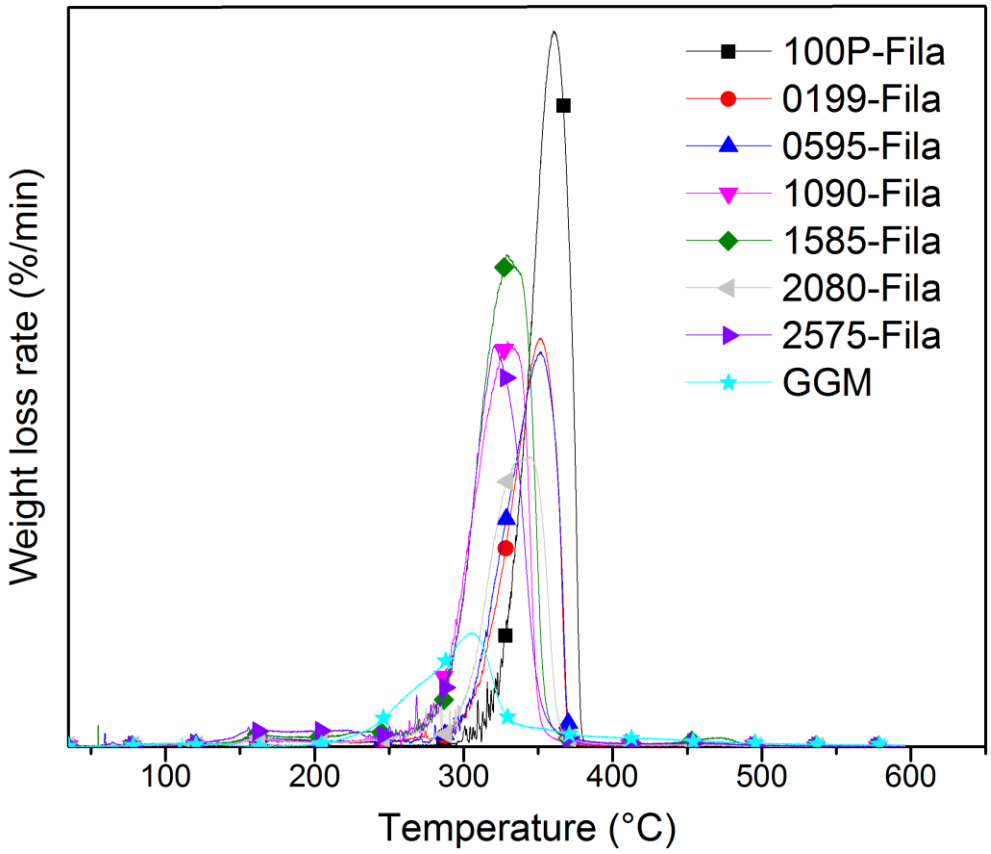

Figure S3. The first derivative thermogravimetric (DTG) curves of the extruded filaments

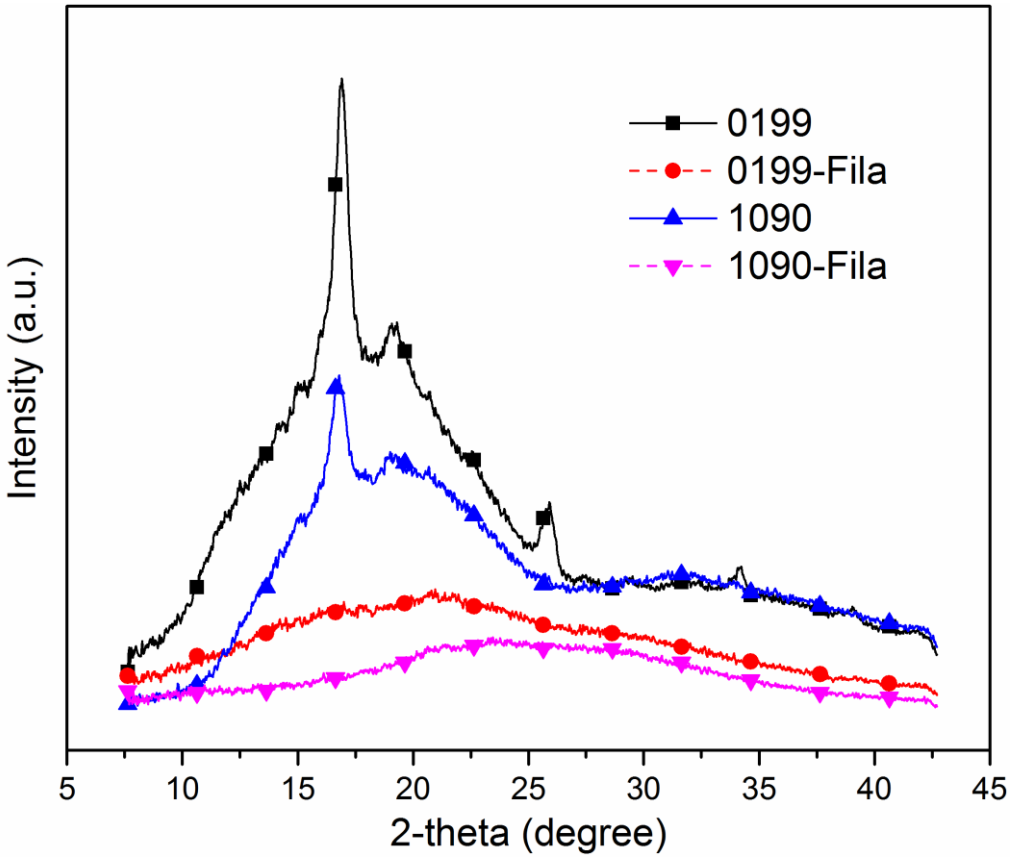

Figure S4. X-ray diffracton pattens for blends and filaments.

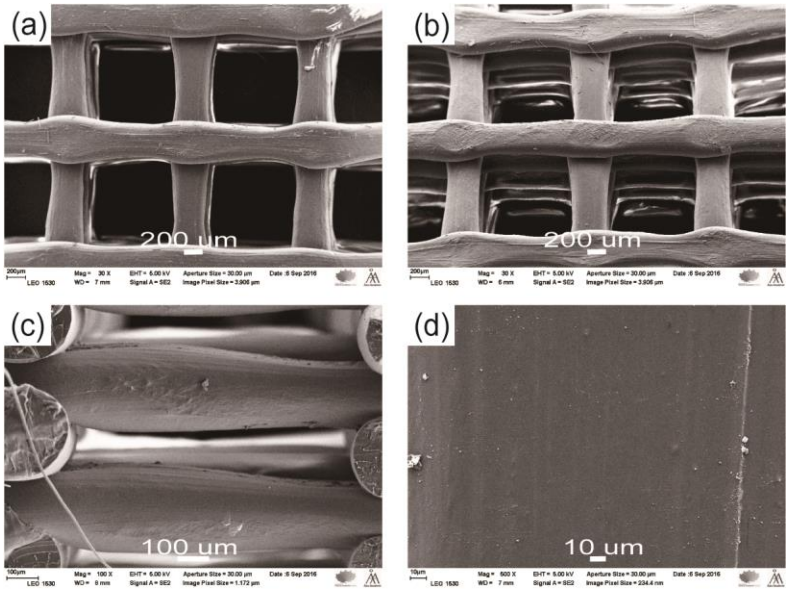

Figure S5. SEM images of 100P-Fila based 3D printed scaffold (a and b),SEM image from side of the scaffold (c), surface image of the 3D printed stripe in the scaffold(d)

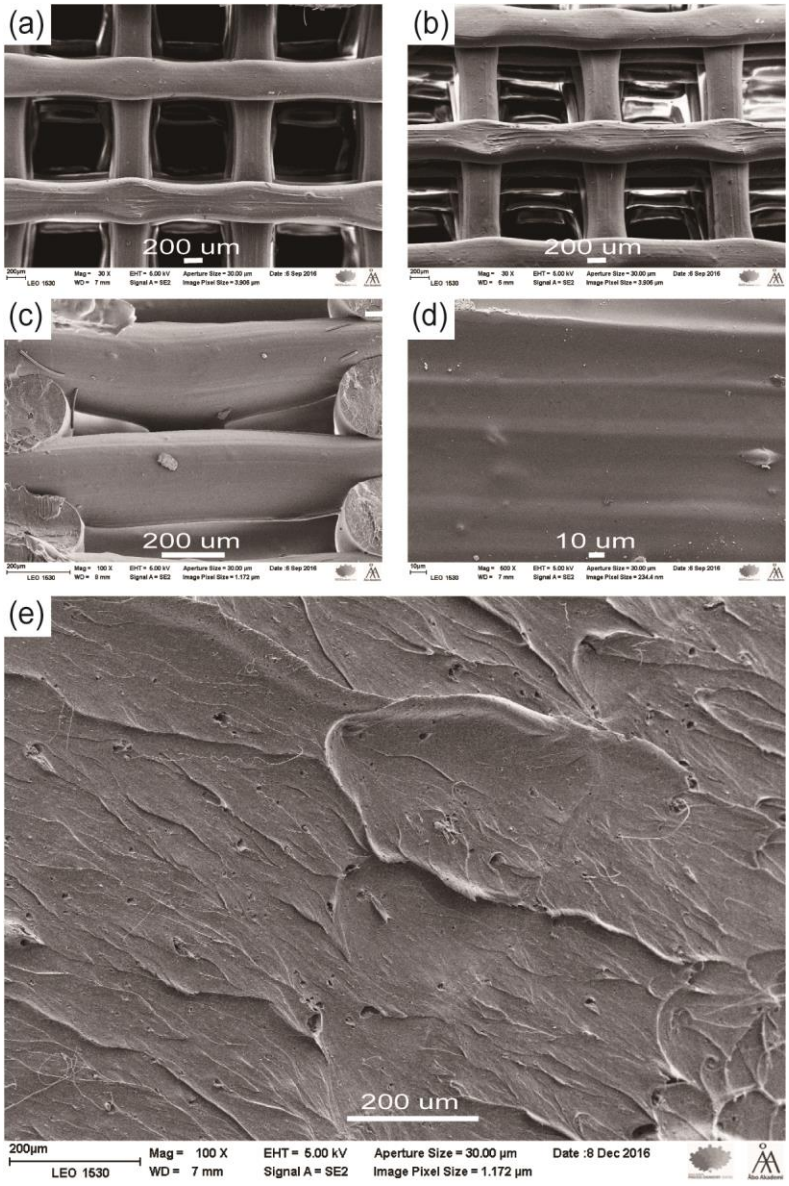

Figure S6. SEM images of 0199-Fila based 3D printed scaffold (a and b),SEM image from side of the scaffold (c), surface image of the 3D printed stripe in the scaffold(d), and bending cross-section images from 0199-Fila (e).

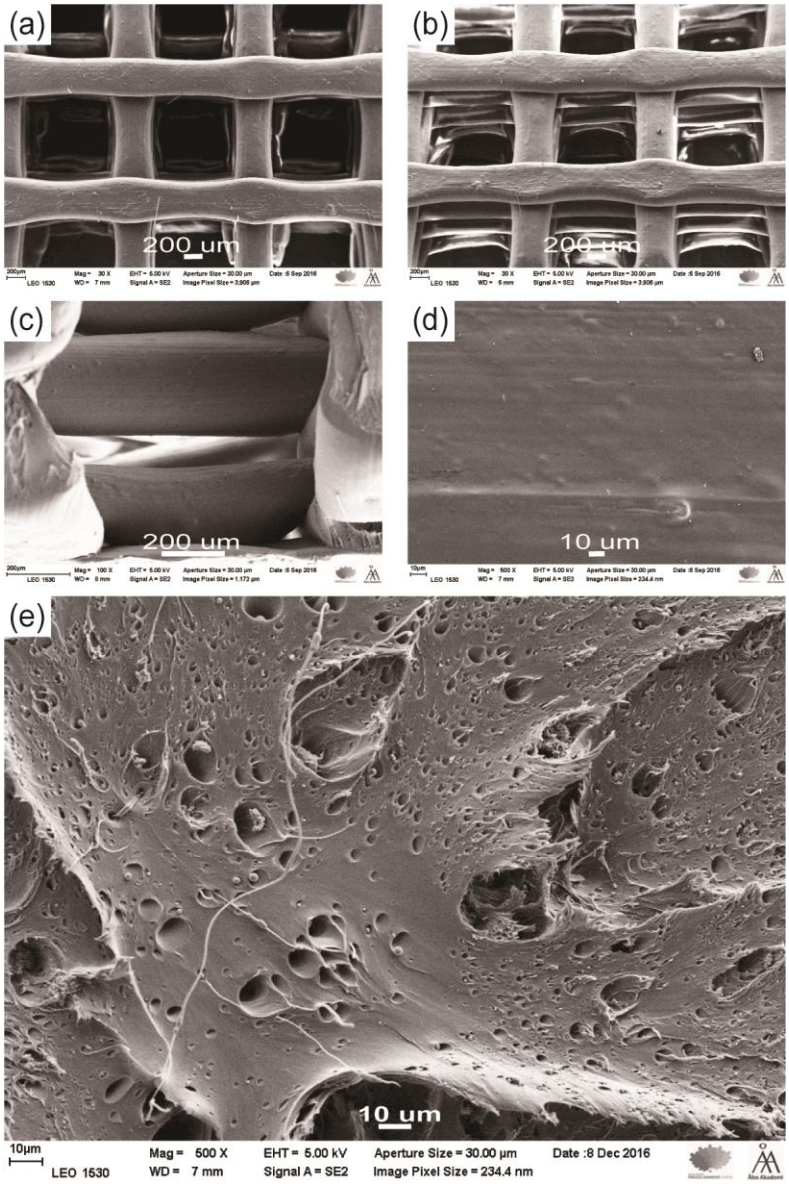

Figure S7. SEM images of 0595-Fila based 3D printed scaffold (a and b),SEM image from side of the scaffold (c), surface image of the 3D printed stripe in the scaffold(d), and bending cross-section images from 0595-Fila (e).

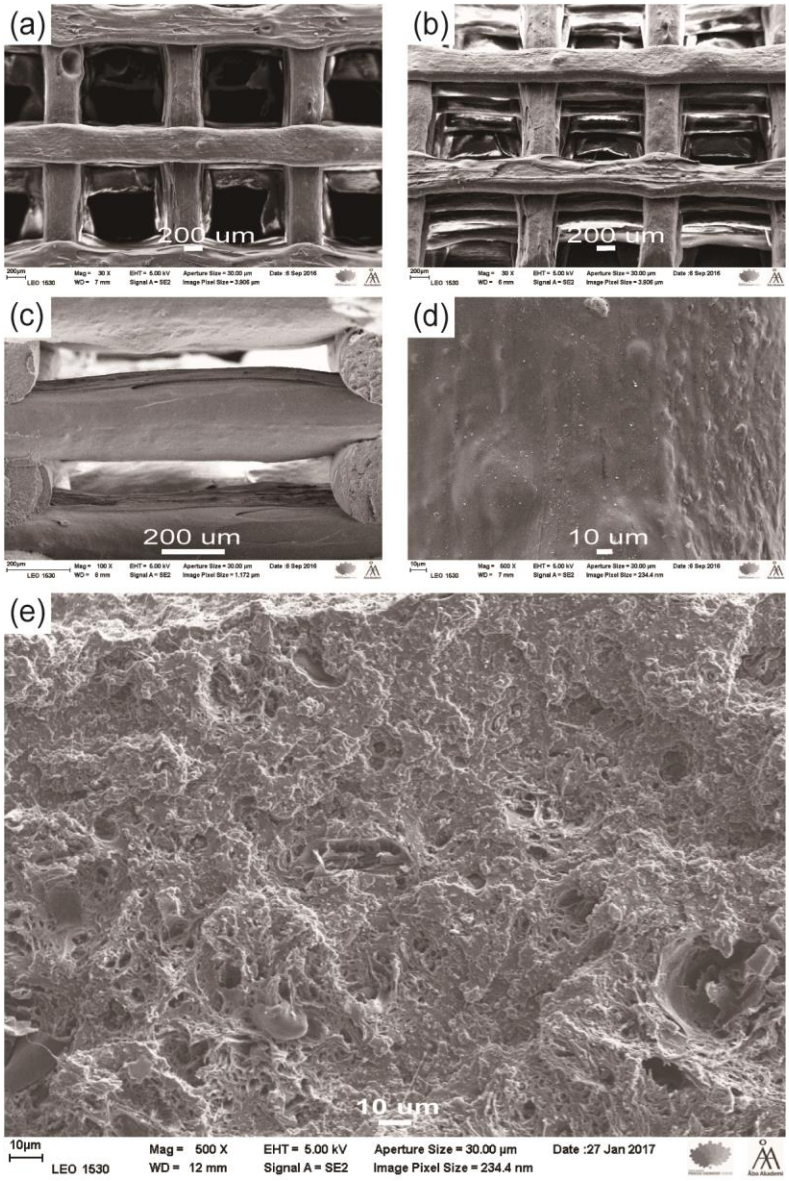

Figure S8. SEM images of 1585-Fila based 3D printed scaffold (a and b),SEM image from side of the scaffold (c), surface image of the 3D printed stripe in the scaffold(d), and bending cross-section images from 1585-Fila (e).

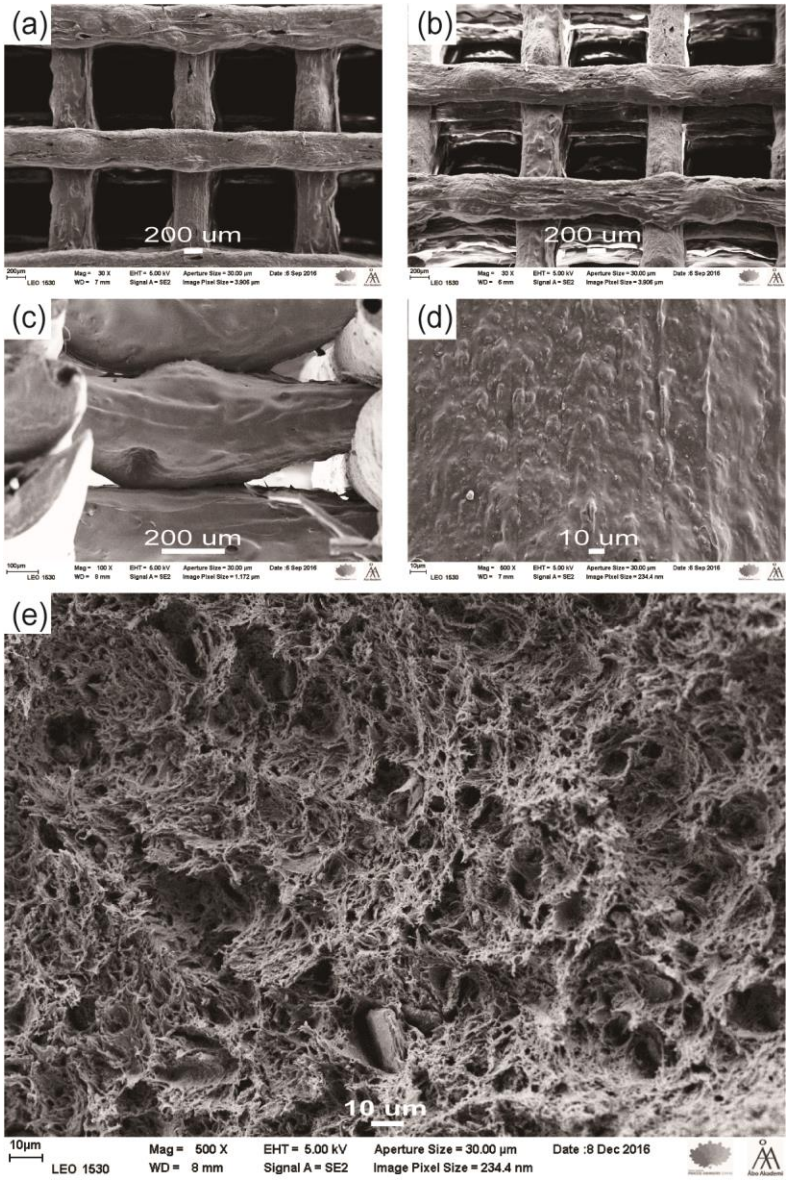

Figure S9. SEM images of 2080-Fila based 3D printed scaffold (a and b),SEM image from side of the scaffold (c), surface image of the 3D printed stripe in the scaffold(d), and bending cross-section images from 2080-Fila (e).

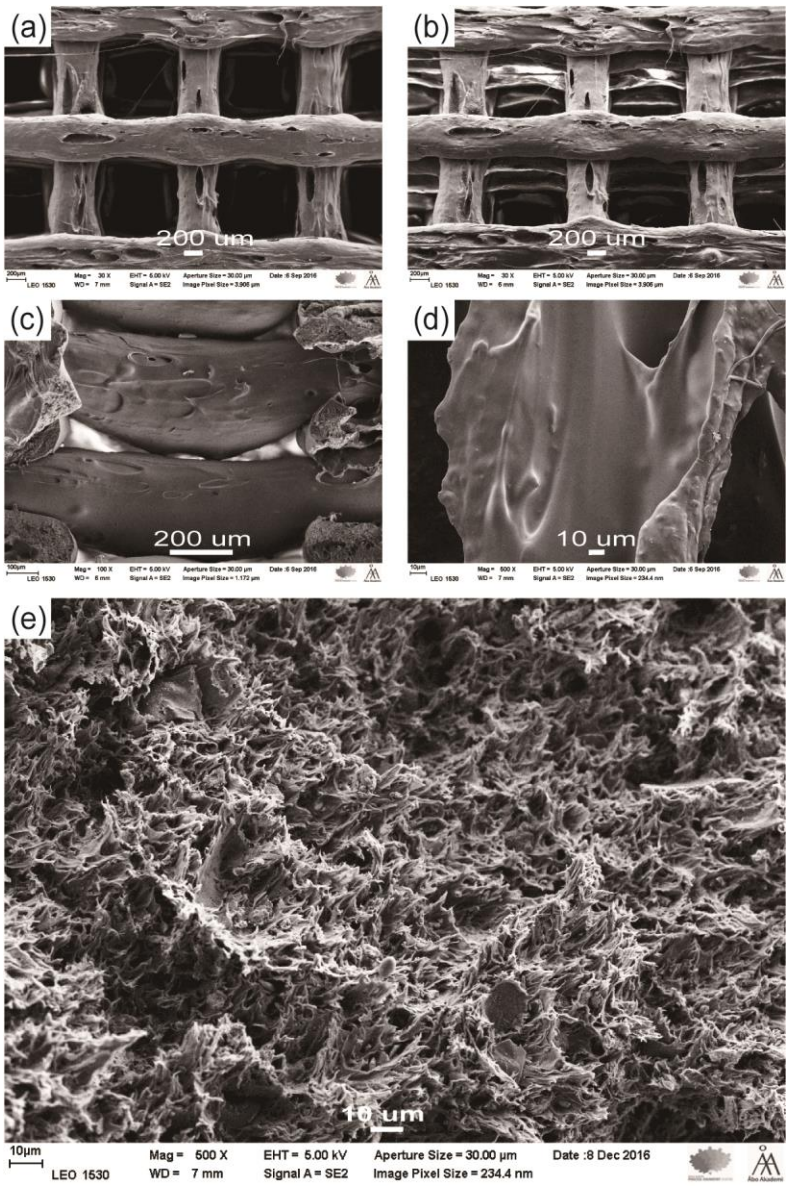

Figure S10. SEM images of 2575-Fila based 3D printed scaffold (a and b),SEM image from side of the scaffold (c), surface image of the 3D printed stripe in the scaffold(d), and bending cross-section images from 2575-Fila (e).

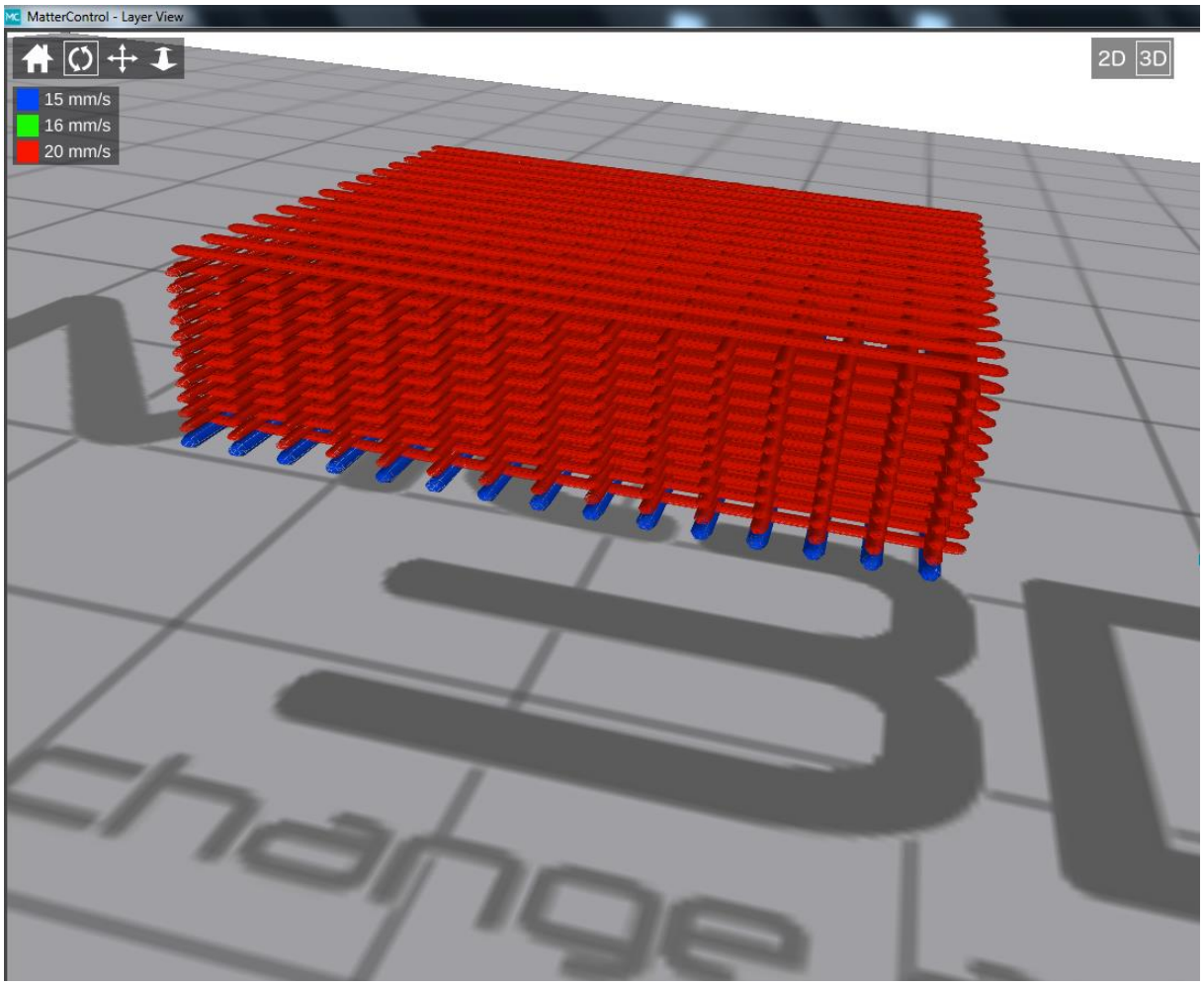

Figure S11. The screenshot of the prototype in MatterControl software